PAPER

Check for updates

A new highly selective "off–on" typical chemosensor of Al³⁺, 1-((Z)-((E)-(3,5-dichloro-2-hydroxybenzylidene)hydrazono)methyl)naphthalene-2-ol, an experimental and *in silico* study†

Jamaludin Al Anshori, [ID] * Daliah Ismalah, Ajar Faflul Abror, Achmad Zainuddin, Ika Wiani Hidayat, Muhammad Yusuf, [ID] Rani Maharani [ID] and Ace Tatang Hidayat

A new promising fluorescent chemosensor based on a 2-hydroxynaphthaldehyde skeleton was successfully synthesized through double imine formation as a yellow solid with an overall chemical yield of 63%. The compound showed UV/Visible maxima of at 394 nm in DMSO. Based on spectroscopic data of FTIR, ToF-HRMS, ^{1}H-NMR, and ^{13}C-NMR, the product was characterized as 1-((Z)-((E)-(3,5-dichloro-2-hydroxybenzilydine)hydrazono)methyl)naphthalene-2-ol. Upon experimental study, the compound was confirmed as a highly selective and reversible off–on typical chemosensor against Al³⁺ with an emission quantum yield of 0.203 ± 0.009. The Job's plot analysis revealed that a highly stable 1:1 complex was formed with an association constant of 8.73×10^5 M^{-1}. A pH-dependent study showed that the sensor was potentially applicable at physiological conditions (pH 7–8) in a mixture of DMSO : H₂O (99 : 1, v/v). The LoD and LoQ of the chemosensor towards Al³⁺ in DMSO were found to be 0.04 and 0.14 μM respectively. Based on DFT and TD-DFT calculation (B3LYP hybrid method/basis set of 6-311+G(d,p)), the sensing mechanism of the chemosensor to the ion was discovered as inhibition of excited-state intramolecular proton transfer (ESIPT).

Introduction

Aluminum is the most abundant metal element in the earth's crust[1,2] and is widely utilized to support human daily needs such as for kitchen ware, electrical apparatus, in the pharmaceutical industry, and also food for packaging materials.[3,4] As a consequence, humans can be exposed easily to Al³⁺ ions for long periods, resulting in slow accumulation in various human organs through food, drugs, and water.[3,5–13] Excessive intake of Al³⁺ ions in the human body may lead to severe diseases such as Alzheimer's,[14,15] Parkinson,[3,16] osteoporosis, osteomalacia,[17] breast cancer,[16,17] amyotrophic lateral sclerosis,[14] neurofibrillary, enzymatic, and neurotransmitter changes in the central nervous system.[18] Thus, early detection of the ions with a proper analysis method becomes urgently necessary, especially for trace analysis of the ions. Such expensive and time-consuming methods for aluminum detection are well established, like graphite furnace atomic absorption spectrometry and

inductively coupled plasma atomic emission spectrometry. Comparatively, optical detection such as the fluorescence method shows unique potential for high sensitivity.[19] At present, fluorescent chemosensors have been widely used to detect different metal ions because of their high sensitivity, selectivity, and fast response time,[20,21] including to detect a trace of Al³⁺ ions. Therefore, the development of an analytical method of Al³⁺ ions based on fluorescence detection is still interesting, in particular, to solve the issues of weak coordination ability of Al³⁺ ions and its lack of spectroscopic characteristics.[16,22–25]

One of the most important and widely explored organic species for its potential applications as a chemosensor is Schiff bases with nitrogen moiety as the chelating centre of metal ions.[13,24,26] Many fluorescent chemosensors of metal ions based on Schiff-base have been designed and examined owing to the simplicity, sensitivity, low-cost, synthetic ease, and strong chelating ability.[23,27,28]

Since the last decade, sensor molecule based on excited-state intramolecular proton transfer (ESIPT) mechanism draws considerable attention because exclusive photophysical properties like extraordinarily large Stokes shifted fluorescence emission without self-reabsorption, and environmental sensitivity.[29] A molecule will experience favourably an ESIPT mechanism if it contains both an acidic (hydrogen donor group) and

Department of Chemistry, Faculty of Mathematics and Natural Sciences, Universitas Padjadjaran, Bandung-Sumedang km.21, Jatinangor, Sumedang, 45363, Indonesia. E-mail: jamaludin.al.anshori@unpad.ac.id

a basic site (hydrogen acceptor group) in proximity leading to keto–enol tautomerization at excited-state.[30] Since the ESIPT process usually occurs on an ultrafast time scale (<100 fs), thus steady-state and femtosecond time-resolved spectroscopy are appropriately utilized to explore the mechanism.[31] However, a DFT/TD-DFT calculation is commonly recommended to study the mechanism instead. In addition, a pre-condition of the ESIPT process such as intramolecular hydrogen bonding and emission changes upon ion chelation could support the theoretical prediction of the mechanism firmly.[31–33] Perhaps, upon combination between an extended Schiff base imine behaving as a hydrogen acceptor and more hydrogen donors, it will not only direct a sensor to an ESIPT process but also improve the spectral properties of the chelated Al^{3+}.

In this article, a new chemosensor with typical extended Schiff base moiety was successfully synthesized. The compound exhibited high selectivity and stability of coordination against Al^{3+} ion. A theoretical study was also performed to investigate the chelating mechanism of the sensor with the ion.

Experimental

Materials and method

The pro analysis grade reagents and solvents, purchased from Sigma Aldrich and Merck, were used. All glassware apparatus was oven-dried before use. ^1H- and ^{13}C-NMR spectra were obtained from Agilent 500 MHz and 126 MHz spectrometers, respectively in $CDCl_3$. The NMR signals were referenced to the residual peak of the (major) solvent. The deuterated solvents were stored over activated 3 Å molecular sieves (8–12 mesh) under dry N_2. UV/Visible absorption spectra and their molar absorptivity were measured on a Shimadzu 8400 UV/Vis spectrometer with matched 1.0 cm quartz cells. The spectra were recorded over 0.1 nm interval data. Emission spectra were recorded on an automated Fluorescence Agilent G9800A Cary Eclipse spectrometer in a 1.0 cm quartz fluorescence cuvettes at 25 °C. The slit of excitation and emission was set to 2.5 nm and 20 nm, respectively while the scanning rate was 600 nm min^{-1}. Each sample was measured at least three times and the spectra were averaged. Infrared spectra were obtained on PerkinElmer FTIR with a potassium bromide (KBr) pellet. Relative masses were recorded on a Mass Spectrometer (Waters High Resolution-Time of Flight-MS Lockspray/HR-TOF-MS) in positive ion mode. The melting points were determined on an uncorrected MP55 electrothermal melting point apparatus in open-end capillary tubes. DFT and TD-DFT calculations[32] were performed on a PC with Processor Intel®Xeon (R) CPU E5-2650 v2@2.60 GHz × 32, RAM 16 GB, Hard disk SSD PCIe, and VGA Zotac GeForce GTX 1080TI AMP EXT CORE. The calculation was performed using the Gaussian 09 program[34] with B3LYP hybrid method[35] and a basis set of 6-311+G(d,p). To achieve the actual condition of experiments, the solvent effect of DMSO was included in the calculations employing Integral Equation Formalism Variant Polarizable Continuum Mode (IEFPCM).[36] Calculation covered such parameters as, structural geometry and spectrum of infra-red, for the mechanism of interaction

study,[36] and gap energy of HOMO–LUMO to study the stability of the chelate compound.[35]

Synthesis of 1-(hydrazonomethyl)naphthalene-2-ol (3)

The precursor of **3** was synthesized based on the method reported by Sousa et al. (2003).[37] Hydrazine monohydrate 98% (0.29 g, 5.69 mmol) and 2-hydroxy-1-napthaldehyde (0.20 g, 1.16 mmol) were dissolved in methanol. The mixture was then stirred for 1.5 hours at ambient temperature. The reaction course was monitored by TLC with an eluent mixture of n-hexane: ethyl acetate (8:2, v/v). A yellowish-red solid was obtained upon solvent evaporation of the reaction mixture with a chemical yield of 92%. The product was directly used for the synthesis of **1** without any further purification. IR spectra (KBr): ν/cm^{-1}; 3390 (weak, O–H), 3250 (weak, NH_2), 3055 (weak, C–H aromatic), 1622 (strong, C=N), and 1580 (strong, C=C aryl) (Fig. SI1†). ToF-HRMS (ES$^+$) m/z: [M−H]$^+$ calculated for $C_{11}H_{11}N_2O$ 187.0866; found 187.0877 (Fig. SI2†).

Synthesis of 1-((Z)-((E)-(3,5-dichloro-2-hydroxybenzilydine) hydrazono) methyl)naphthalene-2-ol (1)

The target compound **1** was designed according to Scheme 1 by referring to analogue procedure reported by Gholizadeh Dogaheh et al. (2017).[38] 1-(hydrazonomethyl)naphthalene-2-ol **3** (0.11 g, 0.62 mmol) was dissolved in a two necks round bottom flask with 30 mL of methanol. 3,5-dichlorobenzaldehyde (0.13 g, 0.68 mmol) was then added stepwise to the reaction flask and stirred. The reaction mixture was further refluxed for 2 hours while employing TLC of silica gel GF-254 and eluent mixture of n-hexane: ethyl acetate (8:2, v/v) to monitor the product formation intermittently. A precipitated product was filtered out and washed with methanol to produce a pure yellow solid with chemical yield of 68%. M.P./ °C: decomposed. UV/Vis spectra in DMSO (5 × 10^{-5} mol dm^{-3}): λ_{max}/nm (ε/mol^{-1} dm^{-3} cm^{-1}): 330 (9420), 394 (13 760) and 494 (4840) (Fig. 1). Emission spectra in DMSO (10^{-5} mol dm^{-3}): $\lambda_{ex}/$ nm; 360, λ_{em}/nm; 593 (Fig. 1). IR spectra (KBr): ν/cm^{-1}; 3074 (medium, C–H sp^2), 1612 (strong, C=N) and 1467 (medium, C=C aryl) (Fig. SI3†). ^1H-NMR (500 MHz, CDCl$_3$): δ_H/ppm; 12.73 (s, 1H); 12.24 (s, 1H); 9.62 (s, 1H); 8.66 (s, 1H) 8.09 (d, J = 8.4 Hz, 1H), 7.90 (d, J = 8.6 Hz, 1H), 7.81 (d, J = 8.0 Hz, 1H), 7.63–7.58 (t, 1H), 7.47 (s, 1H), 7.44–7.40 (t, 1H), 7.27 (s, 1H), 7.23 (d, J = 9.0 Hz, 1H) (Fig. SI4†). ^{13}C-NMR (125 MHz, CDCl$_3$): δ_C/ppm; 107.87; 119.12; 119.24; 119.94; 122.96; 124.27; 124.43; 128.36; 128.55; 129.50; 129.93; 132.75; 132.87; 136.05; 154.22; 161.63; 161.77 and 162.56 (Fig. SI5†). ToF-HRMS (ES$^+$) m/z: [M−H]$^+$ calculated for $C_{18}H_{13}Cl_2N_2O_2$ 359.0349; found 359.0368 (Fig. SI6†).
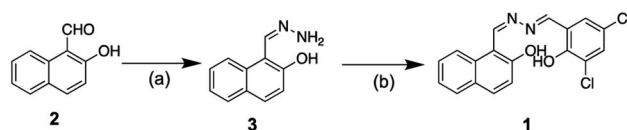
Scheme 1 Outline synthesis route of **1**, 1-((Z)-((E)-(3,5-dichloro-2-hydroxybenzilydine)hydrazono) methyl)naphthalene-2-ol. (a) NH$_2$-NH$_2$·H$_2$O, MeOH, stirred at r.t. for 2 h, (b) 3,5-dichloro-2-hydroxybenzaldehyde, MeOH, refluxed for 2 h.
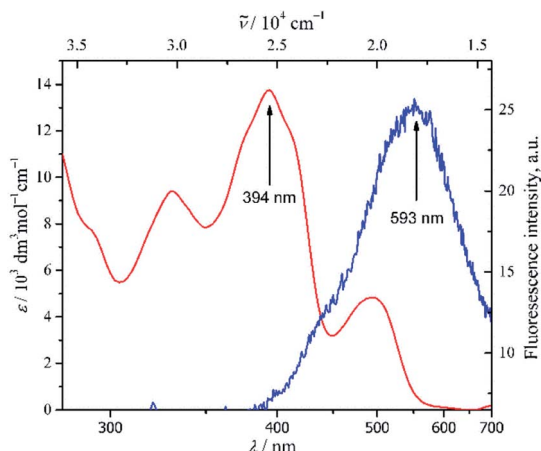
Fig. 1 Spectra of UV/Vis of **1** in DMSO; λ_{max} 394 nm (——) (c_{tot} 5 × 10^{-5} mol dm^{-3}) and emission; λ_{ex} 360 nm, λ_{em} 593 nm (——) (c_{tot} 10^{-5} mol dm^{-3}).

General procedure of metal ion sensing of 1-((Z)-((E)-(3,5-dichloro-2-hydroxybenzilydine)hydrazono) methyl)naphthalene-2-ol (1)

The sensing method was adopted from the reported procedure.[23,39] A stock solution of 1.0×10^{-4} mol dm^{-3} of **1** (**C1**) and metal cationic was prepared in DMSO independently. The representative metal cations were obtained from sulphate salt (K$^+$, Li$^+$, Mg^{2+}, Fe^{3+}, Ni^{2+}, Cu^{2+}, Al^{3+}, Zn^{2+}) and nitrate salt (Na$^+$, Co^{2+}, Cd^{2+}, Hg^{2+}, Pb^{2+}, Ag$^+$). The stock solution of **C1** was mixed with various metal ions in a 5 mL volumetric flask at a mol ratio of 1:9 to 9:1 (**C1**: metal ion) by keeping constant total concentration at 10^{-5} mol dm^{-3}. Binding stoichiometry was calculated based on Job's plot experiment, whilst the selectivity experiment was accomplished by mixing **C1** and Al^{3+} at a mol ratio of 1 : 1 in the presence of each 1 mol of an interference ion. An association constant of the complex calculated with the Benesi–Hildebrand equation[40,41] was obtained from the data of UV-Vis titration experiment of **1** (**C1**) (10 mol dm^{-3}) in the presence of an increasing amount of Al^{3+} (2.4–26 mol dm^{-3}). Whereas the LoD ($3s/k$) and LoQ ($10s/k$)[42] of the **1** toward Al^{3+} were obtained from the data of fluorescence titration experiment of **1** (**C1**) (10^{-5} mol dm^{-3}) in the presence of a gradual amount of Al^{3+} (1.3–16 mol dm^{-3}). The pH effect was studied in DMSO : H$_2$O (99 : 1, v/v) at 10^{-5} mol dm^{-3} using an aqueous solution of NaOH and HCl for pH adjustment. All fluorescence spectra were recorded at an excitation wavelength (λ_{ex}) of 360 nm. The reversibility of the **1** against Al^{3+} was obtained by a fluorescence titration of the **1**+Al^{3+} with EDTA.[43,44] The emission quantum yield (ϕ_{em}) of **1** before and after the addition of Al^{3+} was calculated based on a relative value[43] against a standard of quinine sulphate in 0.5 M of H$_2$SO$_4$ (ϕ_{em} = 0.546).[45]

Result and discussion

Synthesis of 1-((Z)-((E)-(3,5-dichloro-2-hydroxybenzilydine)hydrazono) methyl)naphthalene-2-ol (1)

Upon the formation of a double imine bond *via* addition–elimination reaction of hydrazine to the related aldehyde

precursors, compound **1** was produced straightforwardly with an overall chemical yield of 63% (Scheme 1). Effortlessness synthesis of Schiff base compound[46] was likewise applied to compound **1**. Thus, no further purification was necessary to obtain a pure yellow solid of the product.

The infrared spectra of **1** (Fig. SI3†) showed clearly the appearance of imine moiety by a typical C=N vibration at 1612 cm^{-1} (strong, sharp). The appearance of the aromatic group of naphthalene and substituted benzaldehyde was assigned by the vibration of sp^2 C–H at 3074 cm^{-1} (medium, sharp) and C=C aryl at 1467 cm^{-1} (medium, sharp). However, the sign of –OH moiety was barely apparent, which might be due to intramolecular hydrogen bonding with the nitrogen of imine. To clarify the structure, further analysis of ^{1}H-NMR and ^{13}C-NMR were recorded in CDCl$_3$ (Fig. SI4 and SI5†). Six aromatic protons of naphthalene and two of substituted benzaldehyde had resonance at 7.23–8.10 ppm, whilst two protons of azomethine linkage of Schiff base were revealed at 8.66 ppm and 9.62 ppm. In fact, two more protons signal of –OH group appeared at 12.24 ppm and 12.73 ppm, shifted more downfield than common phenolic proton.[47,48] The shifting of phenolic –OH chemical shift emphasized the probable intramolecular hydrogen bonding occurred, thus it was not distinctive on IR spectra. Furthermore, the intramolecular interaction confirmed the plausible geometry of compound **1**. Supporting the ^{1}H-NMR data, the ^{13}C-NMR analysis revealed 18 distinctive carbon signals. Ten carbons had resonance at 107.87, 119.24, 119.94, 122.96, 128.36, 128.55, 129.50, 132.87, 136.05 and 162.56 ppm, were attributed to naphthalene carbon, whereas the six carbon signals of substituted benzaldehyde were revealed at 119.12, 124.27, 124.43, 129.93, 132.75 and 161.77 ppm. The other two carbons of azomethine were confirmed at 154.22 and 161.63 ppm. Finally, ToF-HRMS confirmed the molecular formula of compound **1** as C$_{18}$H$_{13}$Cl$_2$N$_2$O$_2$ (ES$^+$), which deviated merely 5 ppm from the theoretical mass (Fig. SI6†).

Photophysical properties of compound 1

The absorption spectra of **1** were obtained at 5×10^{-5} mol dm^{-3} in the most polar aprotic solvents of DMSO (Fig. 1). The spectra revealed n → π* characteristic transition bands at λ_{max} 394 nm (13 760 ε/dm^3 mol^{-1} cm^{-1}) and 494 nm (4840 ε/dm^3 mol^{-1} cm^{-1}), which were plausibly attributed to azomethine and phenol moieties respectively. In addition, a π → π* transition band of conjugated aromatic ring and azomethine chromophore was also observed at 330 nm (9420 ε/dm^3 mol^{-1} cm^{-1}). Such a stronger absorption band of n → π* transition than commonly found was might be due to better solvation of polar aprotic DMSO through intermolecular hydrogen bonding, thus allowing to have better stabilization of the compound at the ground state than at the excited state.[49] In fact, upon a less polar aprotic solvent like 1,4-dioxane, just diminished the corresponding n → π* transition band at 494 nm (Fig. SI7†). Further analysis of fluorescence spectra of **1** in DMSO at 10^{-5} mol dm^3 (Fig. 1) asserted the strong interaction between compound **1** with the solvent which quenched significantly emission of the fluorophore of **1**.

Sensing properties of compound 1 against various metal ions

The sensing properties of compound **1** against representative various metal ions including Na^+, K^+, Li^+, Ca^{2+}, Mg^{2+}, Fe^{3+}, Co^{2+}, Ni^{2+}, Cu^{2+}, Cd^{2+}, Hg^{2+}, Pb^{2+}, Ag^+, Al^{3+} and Zn^{2+} were evaluated in DMSO at ambient temperature. Typical metal-induced fluorescence enhancement was demonstrated by **1** in the presence of various metal ions under UV light at 365 nm (Fig. SI8†). In particular, considerable changes of fluorescence intensity of **1** were induced by Al^{3+} ion upon the molar ratio of 1:1 (Fig. 2). The Al^{3+} ion was able to induce the fluorescence of **1** up to one order of magnitude compared to the blank (ϕ_{em} of **1** = 0.020 ± 0.001; ϕ_{em} of **1** + Al^{3+} = 0.203 ± 0.009). In addition, hypsochromic shift emission maxima of **1** + Al^{3+} were also observed up to 152 nm compared to the maxima of **1**. Such an enhanced electronic interaction of Al^{3+} with the core of **1**, containing three coordination moieties, might increase planarity and stability between two aromatic parts of the chelated compound,[50] thus a blue shift was perceived significantly.

Such a fluorophore with Schiff base moieties nearby to any acidic proton like **C1** potentially experienced excited-state intramolecular proton transfer (ESIPT) *via* intramolecular hydrogen bonding[13,51] thus, the fluorescence was quenched. Conversely, upon coordination with Al^{3+} ion, the fluorescence enhancement might be attributed to the ESIPT inhibition process of **C1**, which favoured intramolecular charge transfer (ICT).[52] The aforementioned plausible mechanism was in agreement with other similar Schiff base compounds reported elsewhere.[53,54] Since the value of hydrogen bond-acceptor of DMSO is the strongest one (0.752) among other polar aprotic solvents,[55,56] thereby could assist Al^{3+} ion to disrupt the ESIPT of **C1** compared to other polar aprotic solvents (Fig. SI9†). Further competitive experiment of **1** + Al^{3+} chelated compound against other metal ions revealed that the presence of Al^{3+} ion among other metal ions exhibited immediate response of fluorescence enhancement peculiarly (Fig. 3). Thus, it emphasized the selectivity of **1** towards Al^{3+} and explicitly defined **1** as a typical off–on chemosensor.

To determine binding stoichiometry between **1** and Al^{3+}, Job's plot analyses were employed. Upon keeping the total
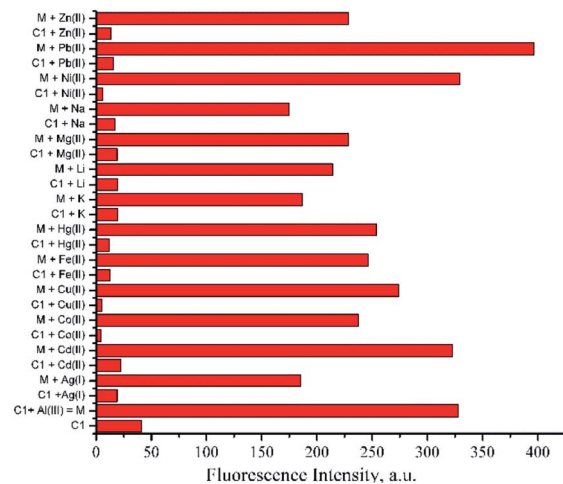

Fig. 3 Selectivity of compound **1** (**C1**) toward Al^{3+} ion in the presence of other metal ions; Ag^+, Cd^{2+}, Co^{3+}, Cu^{2+}, Fe^{3+}, Hg^{2+}, K^+, Li^{2+}, Mg^{2+}, Na^+, Ni^{2+}, Pb^{2+}, Zn^{2+} in DMSO (1 : 1, molar ratio, c_{total} 10^{-5} mol dm^{-3}, λ_{ex} 360 nm, λ_{em} 546 nm).

concentration of the mixture at 10^{-5} mol dm^{-3} and varying the molar ratio of Al^{3+} from 0.1 to 0.9, the complex was found to be firmly established at a molar ratio of 1 : 1 (Fig. 4). In addition, analysis of ToF-HRMS (ES$^+$) showed the exact complex composition of **1** + Al^{3+} as a 1:1 complex (calculated for $C_{18}H_{11}AlCl_2N_2O_2$ 385.0086; found 385.0436) (Fig. SI10†). The aforementioned data was further proved by the high association constant of the complex (8.73 × 10^5 M^{-1}), obtained from the UV-Vis titration experiment and Benesi–Hildebrand equation (Fig. 5).[40,41] The high association constant also confirmed a strong electronic interaction of Al^{3+} with the core of **1**, hence forming a highly stable complex.

A fluorescence titration experiment of **1** in the presence of a gradual amount of Al^{3+} in DMSO was also conducted (Fig. 6). Based on the plotted data assisted by equations of $3s/k$ and $10s/k$,[42] the LoD and LoQ of **1** were found to be 0.04 and 0.14 μM respectively.

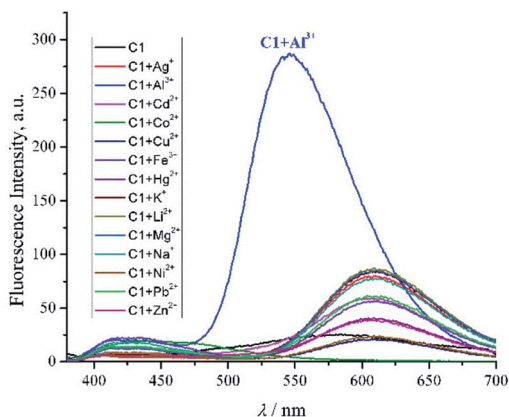**Fig. 2** Emission spectra of compound **1** (**C1**) with the addition of various metal ion (1 : 1, molar ratio) in DMSO (c_{total} 10^{-5} mol dm^{-3}, λ_{ex} 360 nm, λ_{em} 546 nm).
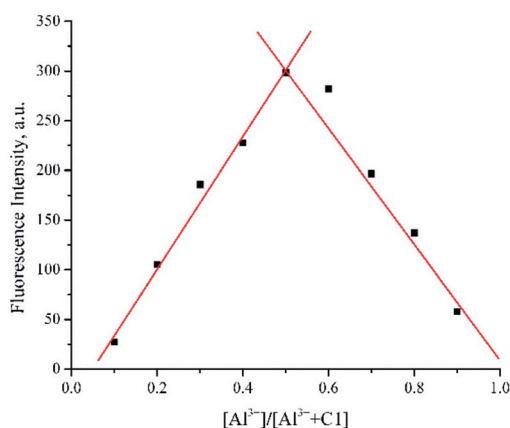

Fig. 4 Job's plot of compound **1** (**C1**) with Al^{3+} in DMSO (c_{total} 10^{-5} mol dm^{-3}, λ_{ex} 360 nm, λ_{em} 546 nm).
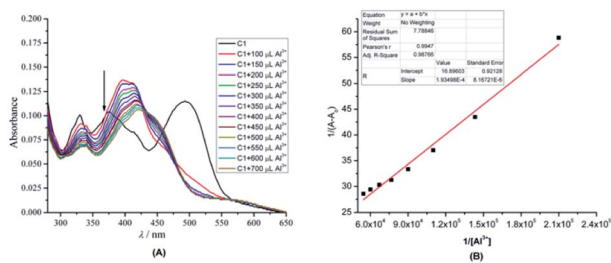
Fig. 5 (A) UV/Vis titration profile of **1** (**C1**) (10 mol dm^{-3}) in the presence of an increasing amount of Al^{3+} (2.4–26 mol dm^{-3}) in DMSO (B) Benesi–Hildebrand plot of **1**.
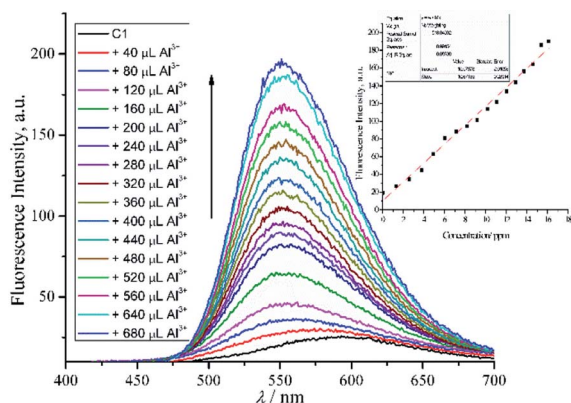

Fig. 6 Fluorescence titration of **1** (**C1**) (10^{-5} mol dm^{-3}; $\lambda_{ex} = 360$ nm) against Al^{3+} ions at room temperature. Inset: plotted fluorescence intensity changes at 546 nm as a function of Al^{3+} concentration.

As compound **1** contained donor and acceptor of an acidic proton within proximity, further study of the interaction between compound **1** and Al^{3+} ion (1 : 1 molar ratio) at various pH was managed with aqueous NaOH or HCl in a mixture of DMSO-H$_2$O (99 : 1, v/v) (Fig. 7). The graph revealed that Al^{3+} + **1** chelated compound exhibited changes of fluorescence intensity at various pH. In particular, the intensity weakened significantly below pH 7 and above pH 9. The faded fluorescence intensity at
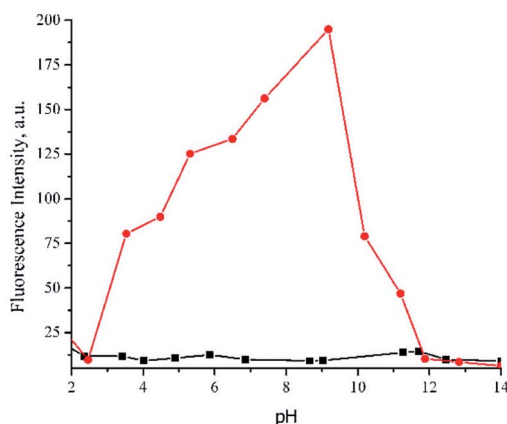
acidic conditions was presumably due to protonated imine Schiff base and phenolic moieties which inhibited **1** to coordinate Al^{3+} ion.[57] On the other hand, upon extremely basic condition, Al^{3+} was plausibly converted to aluminum hydroxide and aluminate anion,[58] allowed the sensor to be free as anionic species in the solution, and finally turned off the emission. Such a pH-dependent typical Schiff base chemosensor, involving an aqueous system, is commonly observed,[43,59,60] especially for the biological application. However, to explore the extensive application of probe **1** under aqueous system domination, further investigation must be conducted. Especially, in terms of the changes of the sensing mechanism in the presence of water which eventually will influence the sensitivity and selectivity. The solvent and molecule symmetry was reported to affect significantly the ESIPT mechanism. In such a case, protic solvent (which undergoes hydrogen bonding) like water could suppress ESIPT by inhibiting keto (K*) emission, hence enol-emission remained at a shorter wavelength.[61] On the other hand, a similar solvent could activate ESIPT and allow to switch on keto (K*) emission[62] by inhibiting photoinduced electron transfer. In spite of that, sensor **1** was very potentially remained applicable at physiological conditions (pH 7–8). The pH study also confirmed the use of probe **1** as a practical sensor in a mixed aqueous medium DMSO-H$_2$O (99 : 1, v/v).

To observe the reversibility of sensor **1** toward Al^{3+}, such a complexing agent like EDTA was used.[43,44] Upon addition of 1 eq of EDTA to a mixture of **1** and Al^{3+}, the fluorescence intensity of **1** + Al^{3+} was reduced substantially and approached the fluorescence profile of **1**. Further addition of excess Al^{3+} (5 eq.) to the previous mixture, recovered the quenched fluorescence of **1** + Al^{3+} in proximity (Fig. 8). The results implied that the **1** + Al^{3+} chelated compound was reversibly dissociated by other complexing agents. Thus, it was potentially reused for certain times.

Computational study of chemosensor mechanism of 1 against Al^{3+} ion

To verify the interaction mechanism of **1** against Al^{3+} ion, DFT and TD-DFT calculations were performed. An *in silico* study (Table 1) revealed changes of bond order of hydrogen of donor

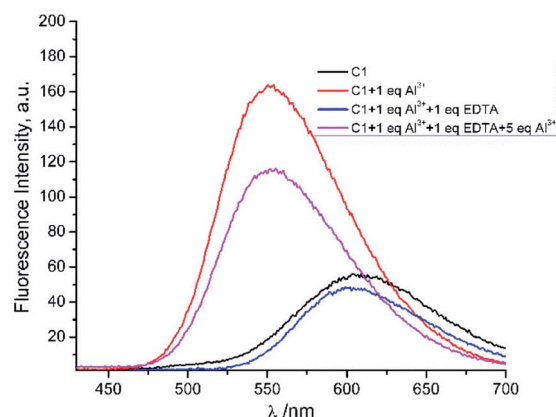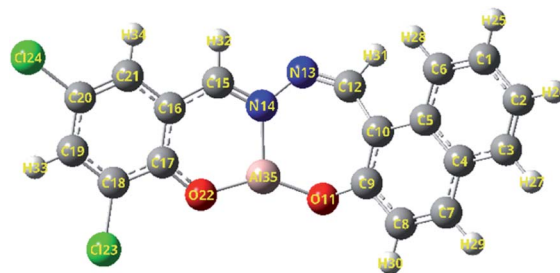**Fig. 7** Effect of pH towards fluorescence intensity of **1** (■) without and (●) with Al^{3+} ion) in DMSO-H$_2$O (99 : 1, v/v).

Fig. 8 The fluorescence reversibility of **1** (**C1**) toward Al^{3+} ($\lambda_{ex} = 360$ nm).

Table 1 The primary bond lengths (Å) of **1**-enol at S_0 and S_1 states in DMSO, calculated by DFT and TD-DFT method at levels of B3LYP/6-31+G(d,p) and TD-B3LYP/6-31+G(d,p)

	Compound **1**-enol/Å	
Bond	S_0	S_1
O22–H35	0.98585	0.97384
O11–H36	0.97451	1.93652
N14–H35	1.81533	1.97098
N14–H36	1.86873	1.02579
N14–O22	2.68221	2.77635
N14–O11	2.77314	2.81878

Fig. 10 Optimized structure Chelated compound of **1**-enol + Al^{3+}.

toward acceptor upon excitation of 1-enol to S_1. The bond order of O11–H36 (1-enol of S_0) was found to stretch up to 0.96201 Å at S_1 (1-enol of S_1) approaching N14. Instead, decreasing a distance of N14–H36 down to 0.84294 Å, tailed by a bond formation sequentially was also observed. Based on optimized geometry of 1-enol (Fig. 9), the stretching vibration of O11–H36 at 3575.90 cm^{-1} was perceptible at S_0 yet undetectable at S_1. In addition, a new stretching vibration of N14–H36 at 3415.25 cm^{-1} appeared at S_1. Accordingly, it validated the existence of proton transfer at an excited state. Overall, the optimized geometry didn't show any negative values of frequency vibration (Table SI1†), which indicated good accordance with calculation. The bond formation of N14–H36 at S_1 should be favourable to occur because of intramolecular hydrogen bonding of O11–H36 and N14 was initially formed at S_0 which eventually triggered an ESIPT at S_1. Such

intramolecular interaction between a hydrogen donor (–OH or –NH$_2$) with a hydrogen acceptor (C=N– or C=O) in proximity less than 2 Å are generally arisen and allowed to undergo ESIPT at an excited state. Consequently, the fluorescence properties are quenched. However, upon strong coordination with an ion-assisted by strong acceptor hydrogen of aprotic solvent like DMSO, the ESIPT is plausibly inhibited, thus turning on back the fluorescence.[51,53,54,63,64] Further study of HOMO–LUMO energy revealed that the gap energy of HOMO–LUMO of **1** decreased significantly up to 0.50 eV upon chelation with Al^{3+} (3.43 eV → 2.93 eV). Such low band gap energy of **1** + Al^{3+} presented good stability of the complex which was displayed in Fig. 10 as a model chelated compound. The calculation was in agreement with the high association constant of the complex obtained from the titration experiment. Overall, the computational study uncovered the interaction mechanism and reinforced the experimental results accordingly.

Conclusions

A new simple Schiff base molecule based on 2-hydroxynaphthaldehyde derivative was successfully synthesized with an overall chemical yield of 63%. The compound demonstrated excellent interaction stability and sensing properties against Al^{3+} selectively. The probe showed good reversibility of sensing and was potentially applicable at physiological conditions (pH 7–8) in a mixture of DMSO : H$_2$O (99 : 1, v/v). The LoD and LoQ of **1** against Al^{3+} in DMSO were 0.04 and 0.14 μM respectively. DFT/TD-DFT calculation confirmed the interaction mechanism of **1** *via* ESIPT inhibition. Thus, the compound was suggested as a potential chemosensor of Al^{3+}.

Author contributions

JA was the main project leader and conceived the overall research idea. JA, DI, and AFA performed the experiments and data collection. AZ, IWH, MY, RM, and ATH were substantially involved in data analysis. DI and AFA drafted the manuscript and JA finalized it. All authors read and approved the final manuscript prior to submission.

Conflicts of interest

There are no conflicts to declare.
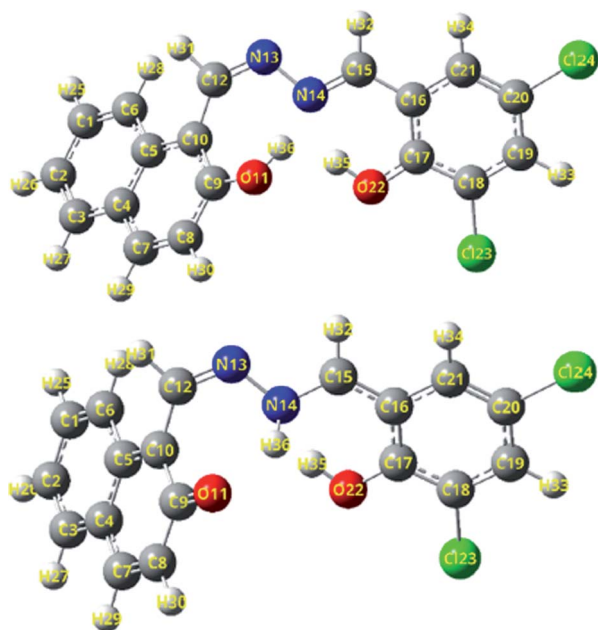
Fig. 9 The optimized structures of **1**-enol form at S_0 and S_1 state, employing a function of B3LYP/TD-B3LYP/6-311+G(d,p) level in DMSO. Top: **1**-enol (S_0) and below: **1**-enol (S_1). Red: oxygen, blue: nitrogen, white: hydrogen, grey: carbon, green: chlor.

Acknowledgements

References

1 D. Maity, S. Dey and P. Roy, *New J. Chem.*, 2017, **41**, 10677–10685.

2 L. Bai, Y. Xu, G. Li, S. Tian, L. Li, F. Tao, A. Deng, S. Wang and L. Wang, *Polymer*, 2019, **11**, 573.

3 B. Naskar, R. Modak, Y. Sikdar, D. K. Maiti, A. Bauzá, A. Frontera, A. Katarkar, K. Chaudhuri and S. Goswami, *Sens. Actuators, B*, 2017, **239**, 1194–1204.

4 F. Liu, C. Fan, Y. Tu and S. Pu, *RSC Adv.*, 2018, **8**, 31113–31120.

5 S. M. Hossain, K. Singh, A. Lakma, R. N. Pradhan and A. K. Singh, *Sens. Actuators, B*, 2017, **239**, 1109–1117.

6 S. Santhi, S. Amala and S. M. Basheer, *J. Chem. Sci.*, 2018, **130**, 1–13.

7 S. Sambamoorthy and A. Subbiah, *Athens J. Sci.*, 2018, **5**, 141–166.

8 R. Azadbakht, T. Almasi, H. Keypour and M. Rezaeivala, *Inorg. Chem. Commun.*, 2013, **33**, 63–67.

9 Y. Li, C. Liao, S. Huang, H. Xu, B. Zheng, J. Du and D. Xiao, *RSC Adv.*, 2016, **6**, 25420–25426.

10 C. Liu, Z. Yang, L. Fan, X. Jin, J. An, X. Cheng and B. Wang, *J. Lumin.*, 2015, **158**, 172–175.

11 Y.-Y. Huang, F.-X. Wang, S.-Y. Mu, X. Sun, Q.-Z. Li, C.-Z. Xie and H.-B. Liu, *Spectrochim. Acta, Part A*, 2020, **15**, 118754.

12 J. Sun, M. Zhang and C. Sun, *Can. J. Chem.*, 2019, **97**, 387–391.

13 M. Tajbakhsh, G. B. Chalmardi, A. Bekhradnia, R. Hosseinzadeh, N. Hasani and M. A. Amiri, *Spectrochim. Acta, Part A*, 2018, **189**, 22–31.

14 C. Chen, D. Liao, C. Wan and A. Wu, *Analyst*, 2013, **2**, 2527–2530.

15 V. K. Gupta, A. K. Singh and L. K. Kumawat, *Sens. Actuators, B*, 2014, **195**, 98–108.

16 Y. W. Choi, G. J. Park, Y. J. Na, H. Y. Jo, S. A. Lee, G. R. You and C. Kim, *Sens. Actuators, B*, 2014, **194**, 343–352.

17 R. Azadbakht and S. Rashidi, *Spectrochim. Acta, Part A*, 2014, **127**, 329–334.

18 T. Jia, W. Cao, X. Zheng and L. Jin, *Tetrahedron Lett.*, 2013, **54**, 3471–3474.

19 R. Azadbakht, T. Almasi, H. Keypour and M. Rezaeivala, *Inorg. Chem. Commun.*, 2013, **33**, 63–67.

20 J. Xu, H. Li, L. Li, J. Wang, F. Wang and L. He, *J. Braz. Chem. Soc.*, 2020, **31**, 1778–1786.

21 J. Al-Anshori, A. Rahim, A. Abror, I. Hidayat, T. Mayanti, M. Yusuf, J. Juliandri and A. Hidayat, *J. Serb. Chem. Soc.*, 2021, **86**, 971–982.

22 S. Banerjee, *RSC Adv.*, 2016, **6**, 101924–101936.

23 C. Sun, X. Miao, L. Zhang, W. Li and Z. Chang, *Inorg. Chim. Acta*, 2018, **478**, 112–117.

24 N. Roy, H. A. R. Pramanik, P. C. Paul and S. T. Singh, *J. Fluoresc.*, 2014, **24**, 1099–1106.

25 J. C. Qin, Z. Y. Yang and P. Yang, *Inorg. Chim. Acta*, 2015, **432**, 136–141.

26 J. C. Qin, Z. Y. Yang and P. Yang, *Inorg. Chim. Acta*, 2015, **432**, 136–141.

27 H. Shekaari, A. Kazempour and M. Khoshalhanc, *Phys. Chem. Chem. Phys.*, 2015, **17**, 2179–2191.

28 K. Zhang, Z. Y. Yang, B. D. Wang, S. B. Sun, Y. D. Li, T. R. Li, Z. C. Liu and J. M. An, *Spectrochim. Acta, Part A*, 2014, **124**, 59–63.

29 A. Gupta and N. Kumar, *RSC Adv.*, 2016, **6**, 106413–106434.

30 H. Tian, X. Qiao, Z.-L. Zhang, C.-Z. Xie, Q.-Z. Li and J.-Y. Xu, *Spectrochim. Acta, Part A*, 2019, **207**, 31–38.

31 P. Zhou and K. Han, *Acc. Chem. Res.*, 2018, **51**, 1681–1690.

32 J.-S. Chen, P.-W. Zhou, L. Zhao and T.-S. Chu, *RSC Adv.*, 2014, **4**, 254–259.

33 N. Zhao, Y. Li, Y. Jia and P. Li, *J. Phys. Chem. C*, 2018, **122**, 26576–26583.

34 M. J. Frisch, G. Trucks, H. B. Schlegel, G. E. Scuseria, M. A. Robb, J. R. Cheeseman, G. Scalmani, V. Barone, G. A. Petersson, H. Nakatsuji, X. Li, M. Caricato, A. V Marenich, J. Bloino, B. G. Janesko, R. Gomperts, B. Mennucci, H. P. Hratchian, J. V Ortiz, A. F. Izmaylov, J. L. Sonnenberg, Williams, F. Ding, F. Lipparini, F. Egidi, J. Goings, B. Peng, A. Petrone, T. Henderson, D. Ranasinghe, V. G. Zakrzewski, J. Gao, N. Rega, G. Zheng, W. Liang, M. Hada, M. Ehara, K. Toyota, R. Fukuda, J. Hasegawa, M. Ishida, T. Nakajima, Y. Honda, O. Kitao, H. Nakai, T. Vreven, K. Throssell, J. A. Montgomery Jr, J. E. Peralta, F. Ogliaro, M. J. Bearpark, J. J. Heyd, E. . Brothers, K. N. Kudin, V. N. Staroverov, T. A. Keith, R. Kobayashi, J. Normand, K. Raghavachari, A. P. Rendell, J. C. Burant, S. S. Iyengar, J. Tomasi, M. Cossi, J. M. Millam, M. Klene, C. Adamo, R. Cammi, J. W. Ochterski, R. L. Martin, K. Morokuma, O. Farkas, J. B. Foresman and D. J. Fox, https://gaussian.com, 2016.

35 I. Abdulazeez, C. Basheer and A. A. Al-Saadi, *RSC Adv.*, 2018, **8**, 39983–39991.

36 S. Su and H. Fang, *Spectrochim. Acta, Part A*, 2020, **233**, 118214.

37 C. Sousa, C. Freire and B. De Castro, *Molecules*, 2003, **12**, 894–900.

38 S. Gholizadeh Dogaheh, H. Khanmohammadi and E. C. Sañudo, *Polyhedron*, 2017, **133**, 48–53.

39 M. Amirnasr, R. Sadeghi Erami and S. Meghdadi, *Sens. Actuators, B*, 2016, **233**, 355–360.

40 K. C. Tayade, A. S. Kuwar, U. A. Fegade, H. Sharma, N. Singh, U. D. Patil and S. B. Attarde, *J. Fluoresc.*, 2014, **24**, 19–26.

41 Y. He, J. Yin and G. Wang, *Chem. Heterocycl. Compd.*, 2018, **54**, 146–152.

42 Q. Zhang, Q. Jiao, Q. Zhang and Z. Liu, *Spectrochim. Acta, Part A*, 2019, **211**, 1–8.

43 J. Tian, X. Yan, H. Yang and F. Tian, *RSC Adv.*, 2015, **5**, 107012–107019.

44 S. M. Hossain, K. Singh, A. Lakma, R. N. Pradhan and A. K. Singh, *Sens. Actuators, B*, 2017, **239**, 1109–1117.

45 A. Brouwer, *Pure Appl. Chem.*, 2011, **83**, 2213–2228.

46 A. Kundu, P. S. Hariharan, K. Prabakaran and S. P. Anthony, *Spectrochim. Acta, Part A*, 2015, **151**, 426–431.

47 P. Charisiadis, V. G. Kontogianni, C. G. Tsiafoulis, A. G. Tzakos, M. Siskos and I. P. Gerothanassis, *Molecules*, 2014, **19**, 13643–13682.

48 P. E. Hansen and J. Spanget-Larsen, *Molecules*, 2017, **22**, 552.

49 A. Mohammadi and J. Jabbari, *Can. J. Chem.*, 2016, **94**, 631–636.

50 Z. Ning, S. Xuan, F. R. Fronczek, K. M. Smith and M. G. H. Vicente, *J. Org. Chem.*, 2017, **82**, 3880–3885.

51 A. Grupta, *RSC Adv.*, 2016, **6**, 106413–106434.

52 G. Dhaka, N. Kaur and J. Singh, *J. Photochem. Photobiol., A*, 2017, **335**, 174–181.

53 H.-Y. Lin, P.-Y. Cheng, C.-F. Wan and A.-T. Wu, *Analyst*, 2012, **137**, 4415–4417.

54 L. Yang, W. Zhu, M. Fang, Q. Zhang and C. Li, *Spectrochim. Acta, Part A*, 2013, **109**, 186–192.

55 M. J. Kamlet and R. W. Taft, *J. Am. Chem. Soc.*, 1976, **98**, 377–383.

56 M. J. Kamlet, J. L. M. Abboud, M. H. Abraham and R. W. Taft, *J. Org. Chem.*, 1983, **48**, 2877–2887.

57 T. S. Singh, P. C. Paul and H. A. R. Pramanik, *Spectrochim. Acta, Part A*, 2014, **121**, 520–526.

58 Z. Salarvand, M. Amirnasr and S. Meghdadi, *J. Lumin.*, 2019, **207**, 78–84.

59 D. Maity, S. Dey and P. Roy, *New J. Chem.*, 2017, **41**, 10677–10685.

60 C. Hazneci, K. Ertekin, B. Yenigul and E. Cetinkaya, *Dyes Pigm.*, 2004, **62**, 35–41.

61 S. Sharma and K. S. Ghosh, *Spectrochim. Acta, Part A*, 2021, **254**, 119610.

62 L. McDonald, J. Wang, N. Alexander, H. Li, T. Liu and Y. Pang, *J. Phys. Chem. B*, 2016, **120**, 766–772.

63 M. Tajbakhsh, *Spectrochim. Acta, Part A*, 2018, **189**, 22–31.

64 A. C. Sedgwick, L. Wu, H. H. Han, S. D. Bull, X. P. He, T. D. James, J. L. Sessler, B. Z. Tang, H. Tian and J. Yoon, *Chem. Soc. Rev.*, 2018, **47**, 8842–8880.